Oxidation of Metals, Vol. 27, Nos. 5/6, 1987

Oxidation of Iron–Silicon Alloys

T. Adachi*† and G. H. Meier*

Received October 22 1986

The isothermal and cyclic oxidation behavior of Fe–Si alloys (5, 10, 14, and 20 wt.% Si) was studied between 900 and 1100°C. The oxidation rate in air decreased with increasing Si content at all temperatures. Alloys containing 10% Si or more oxidized slower than a typical Cr_2O_3-forming alloy due to the formation of an SiO_2 film. This film may have initially been vitreous but was crystalline after short times. The oxidation kinetics, although slow, were linear due to the outward transport of Fe through the slowly growing SiO_2 film. It is hypothesized that the Fe transport involved atoms rather than ions. Cyclic oxidation behavior varied with the alloy Si content.

KEY WORDS: oxidation; Fe-base alloys; silica.

INTRODUCTION

The oxidation behavior of Fe-Si alloy has been the subject of numerous investigations[1–7]. In a number of cases, the addition of Si to Fe in sufficient amounts to form an external film of SiO_2 or other Si-rich oxide has resulted in extremely slow oxidation rates. In addition, Si additions have been observed to increase the resistance of ferrous alloys to carburization[8] and sulfidation.[9] Atkinson[10] analyzed the selective oxidation behavior of Fe-Si alloys and predicted the Si concentrations required to develop and maintain protective SiO_2 films as a function of temperature. This analysis predicts that atom fractions of Si in Fe of approximately 0.05 and 0.055 are required

*Department of Materials Science and Engineering, University of Pittsburgh, Pittsburgh, Pennsylvania 15261.
†On leave from Nippon Yakin Kogyo Co., Ltd, 4-2 Kojima-Cho, Kawasaki-Ku, Kawasaki-City Kanagawa, Japan 210.

Table I. Composition and Phases of Iron–Silicon Alloys

Nominal composition	Fe. 5 wt.% Si	Fe. 10 wt.% Si	Fe. 14 wt.% Si	Fe. 20 wt. % Si
Actual composition	5.34 wt.% Si	10.83 wt. % Si	13.43 wt.% Si	19.79 wt.% Si
Phases	α-phase	α or β_2[a]	$(\alpha)Fe_3Si$	$Fe_3Si + Fe_5Si_3$[b]
Structure	bcc	bcc, ordered bcc (B2)	Cubic (DO_3)	Cubic hexagonal

[a]X-ray diffraction (XRD) data were not conclusive to distinguish α and β_2.
[b]Only Fe_5Si_3 was clearly detected by XRD, but scanning electron microscopic analysis showed that this alloy consists of two phases, and the composition of the other phase was the same as Fe_3Si.

at 1000°C and 900°C, respectively. The present study involves the isothermal and cyclic oxidation behavior of Fe–Si alloys containing 5–20 wt.% Si in air at temperatures of 900–1100°C.

EXPERIMENTAL

Specimen Preparation

Iron–silicon alloys were arc melted under a purified argon atmosphere and drop cast into a water-cooled copper chill of dimensions 150 × 25 × 9 mm. The nominal compositions of the alloys were 5, 10, 14, and 20 wt.% Si. The analyzed compositions are given in Table I. (Alloys are referred to by nominal compositions in the text.) The ingots were homogenized in purified argon for 150 hr at 1100°C. The phases present, as indicated by X-ray diffraction, are also listed in Table I. The phases were essentially consistent with the published phase diagrams[11,12] for the Fe–Si system as seen from the Fe-rich portion of Fig. 1.[11] The diffracted intensities for Fe–10Si were not sufficient to distinguish between the disordered α-phase, indicated to be stable at 1100°C,[11] and the ordered β_2-phase.[12] Specimens of dimensions 11 × 8 × 2 mm for isothermal oxidation and 22 × 8 × 2 mm for cyclic oxidation were cut from the ingots, polished through 600-grit SiC, and cleaned in alcohol and acetone prior to oxidation.

Oxidation Exposure

Isothermal oxidation tests were run in air and in argon ($p_{O_2} \simeq 10^{-4}$ atm) for times as long as 1 week at 900, 1000, and 1100°C. The weight change of the specimens was measured continuously using a Cahn 2000 microbalance.

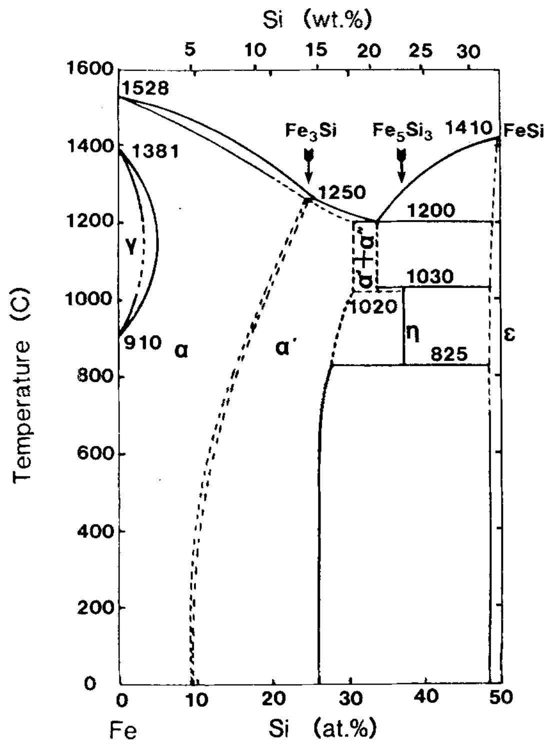

Fig. 1. Iron-rich portion of the Fe–Si phase diagram.[11]

Cyclic oxidation tests were run in air for up to 1075 cycles at 900, 1000, and 1100°C. Each cycle consisted of 45 min at temperature and 15 min cooling at room temperature.

Acoustic Emission Experiments

Selected specimens were monitored by acoustic emission (AE) during oxidation in air at 1100°C and during cooling to detect scale cracking. The AE apparatus and test procedure were those used by Ashary *et al.*,[13] except that the Pt waveguide was replaced by an alumina waveguide described by Perkins and Meier.[14]

Analysis of Oxidation Products

The phases present in the oxide scales were determined by X-ray diffraction using both the diffractometer and Debye–Scherrer powder method. The morphology and composition of the oxidation products were

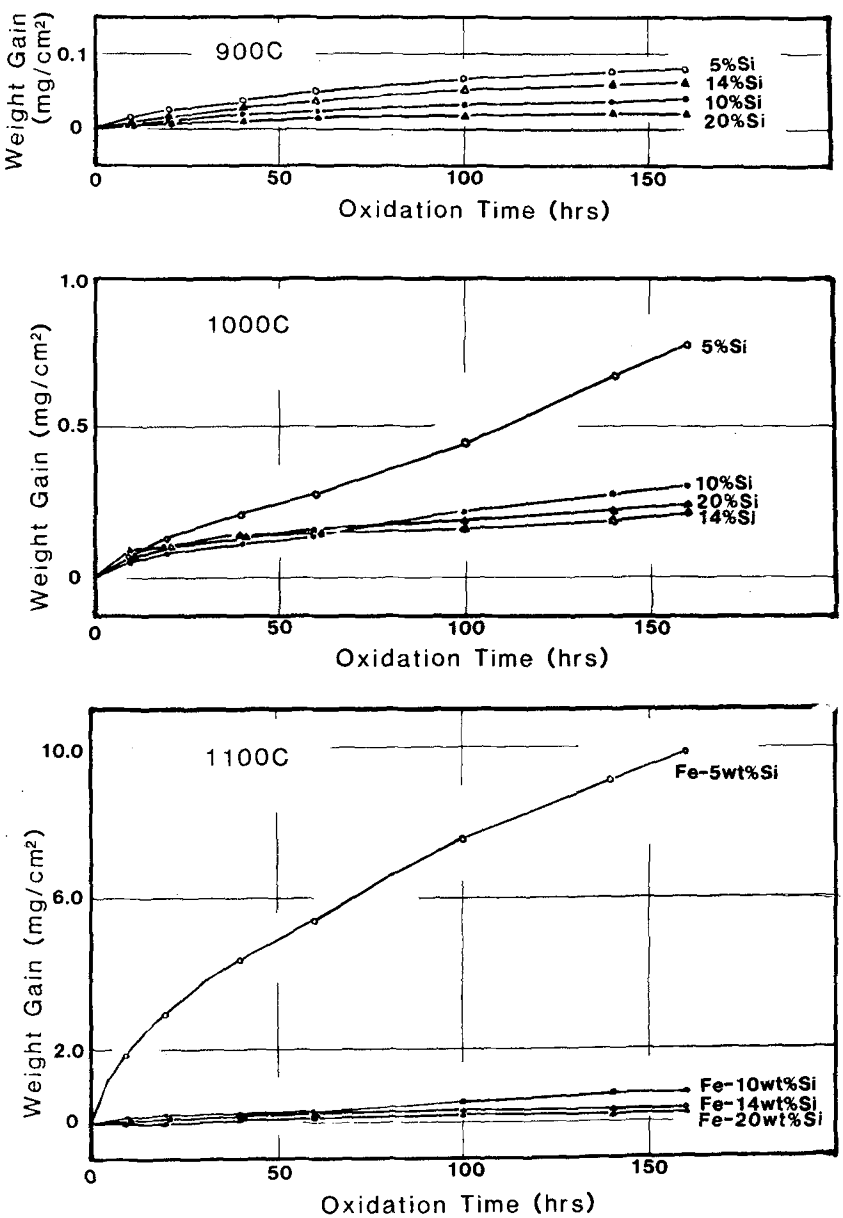

Fig. 2. Isothermal oxidation rates (weight change vs time) for Fe-Si alloys in air.

studied using scanning electron microscopy (SEM) and energy-dispersive X-ray (EDX) analysis.

RESULTS AND DISCUSSION

Isothermal Oxidation

Weight gain-versus-time curves for the four alloys exposed in air are shown in Fig. 2 for the three temperatures studied. The 150-hr weight gains of the alloys at 1100°C are compared in Table II with those of pure Fe[15] and Fe–26Cr[16], an alloy that forms a protective layer of Cr_2O_3. The addition of 5 wt.% Si is observed to decrease the oxidation rate of Fe by more than two orders of magnitude and 10 or more wt.% Si results in oxidation rates slower than that of Fe–Cr. At 900°C, the weight change vs. time curves are essentially parabolic for all four Fe–Si alloys with 150-hr weight gains of less than 0.1 mg/cm^2. At 1000 and 1100°C, the weight gains are correspondingly larger and the weight change-versus-time curves become essentially linear after a short initial period even for the alloys with the slowest oxidation rate.

The oxides detected in the scales by X-ray diffraction after oxidation at 1100°C are indicated in Table III and the oxidation morphologies are presented in Figs. 3–6. Figure 3 shows the scale–gas interface for alloys oxidized for 1 hr. The scale on Fe–5Si consists mainly of Fe_2O_3 with small amounts of Si-rich oxide which appear as dark, smooth areas. The scale on Fe–10Si was comprised mainly of the dark, smooth oxide and islands of Fe_2O_3. Both Fe–14Si and Fe–20Si were covered with the Si-rich oxide. The scale formed numerous cracks on cooling on Fe–14Si but not on Fe–20Si. The Si-rich oxides were too thin after 1 hr for identification by X-ray diffraction but were identified as cristobalite after 4 hr oxidation at 1100°C. This phase remained untransformed on Fe–14Si and Fe–20Si after

Table II. Comparison of 150 hr Weight Gains for Several Ferrous Alloys at 1100°C

Alloy	Weight gain (mg/cm^2)	Ref.
Pure Fe	1046	15
Fe–26Cr	2	1
Fe–5Si	9	This study
Fe–10Si	0.9	This study
Fe–14Si	0.5	This study
Fe–20Si	0.4	This study

Table III. Oxide Scale Formed on Fe–Si Alloys at 1100°C

Oxidation/Si time Content	5 wt.%	10 wt.%	14 wt.%	20 wt.%
1 hr	Fe_2O_3	$Fe_2O_3 + SiO_2$[a]	SiO_2[a]	SiO_2[a]
4 hr	Fe_2O_3	Fe_2O_3 + Cristo	Cristo[b]	Fe_2O_3 + Cristo
24 hr	Fe_2O_3	Fe_2O_3 + Tridy[c]	Fe_2O_3 + Cristo	Fe_2O_3 + Cristo
1 week	$Fe_2O_3 + Fe_2SiO_4$	$Fe_2 + O_3 + Fe_3O_4$	Fe_2O_3 + Cristo	Fe_2O_3 + Cristo

[a]The structure of SiO_2 is unknown, because the thickness of the scale was too thin to be detected by X-ray diffraction.
[b]Cristo, Cristobalite.
[c]Tridy, Tridymite.

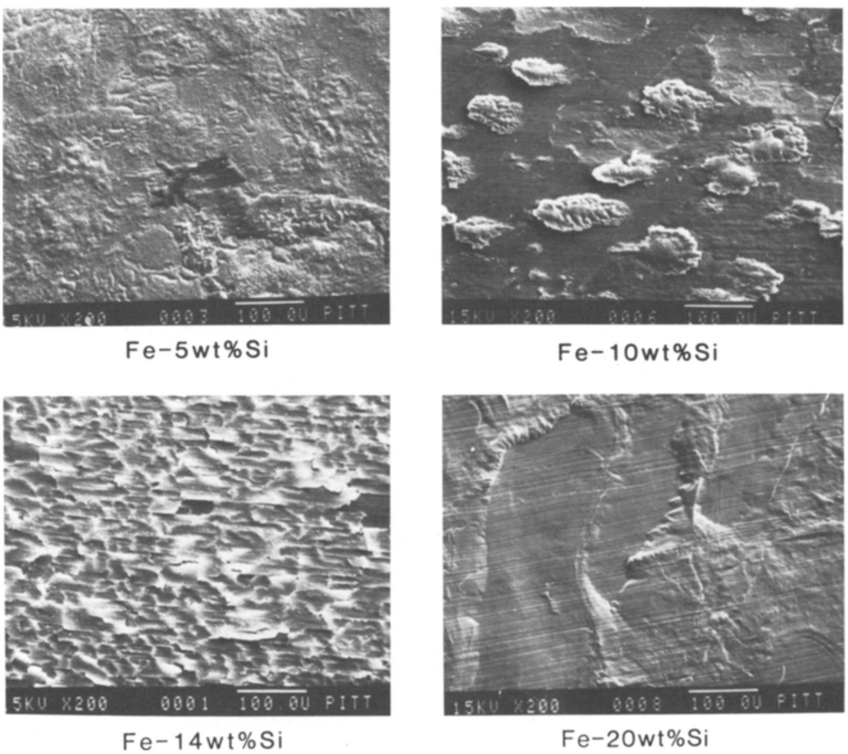

Fig. 3. Scale gas interfaces of Fe–Si alloys oxidized in air for 1 hr at 1100°C.

oxidation times as long as 150 hr but transformed to tridymite after 24 hr on Fe-10Si. The initial formation of SiO_2 on Fe-Si alloys has been reported to involve a vitreous oxide[1] and vitreous SiO_2 has been identified by transmission electron microscopy (TEM) on Ni-Si alloys after 1 hr oxidation at 950°C.[9] Therefore, the cristobalite observed in the present study is likely the product of devitrification of a vitreous film that forms as an intermediate product before transformation to tridymite, which is the most stable form of SiO_2 in this temperature range.

Figure 4 shows the surface and cross section of three alloys oxidized for 1 week at 1100°C. The scale on Fe-5Si consists of a thick outer layer

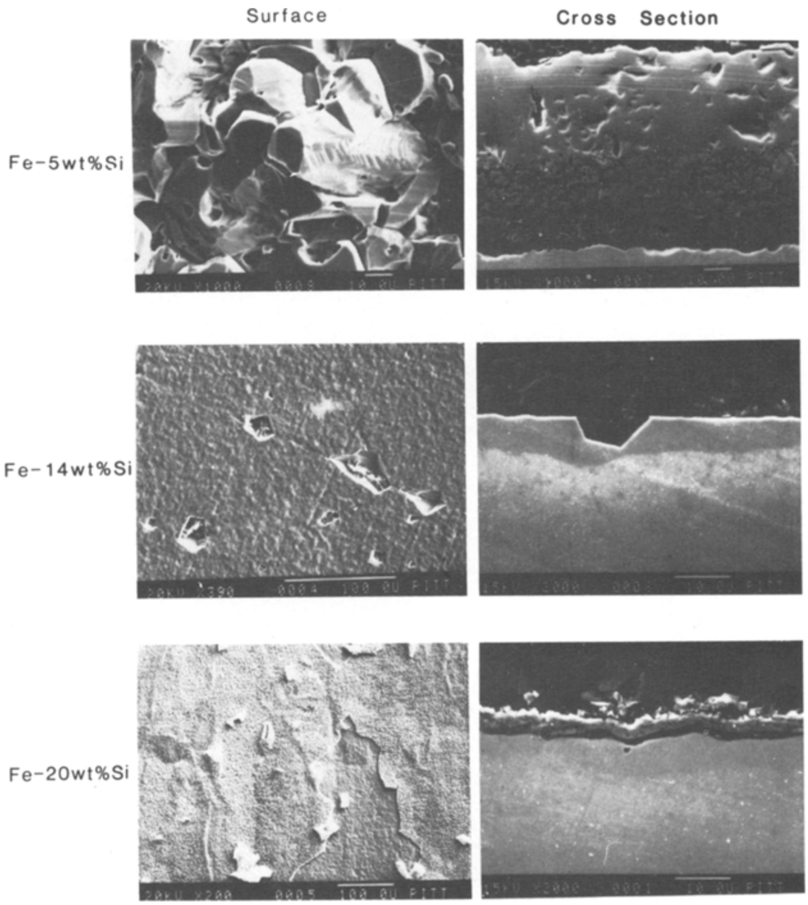

Fig. 4. Scale/gas interface and cross section for three Fe-Si alloys oxidized in air for 1 week at 1100°C.

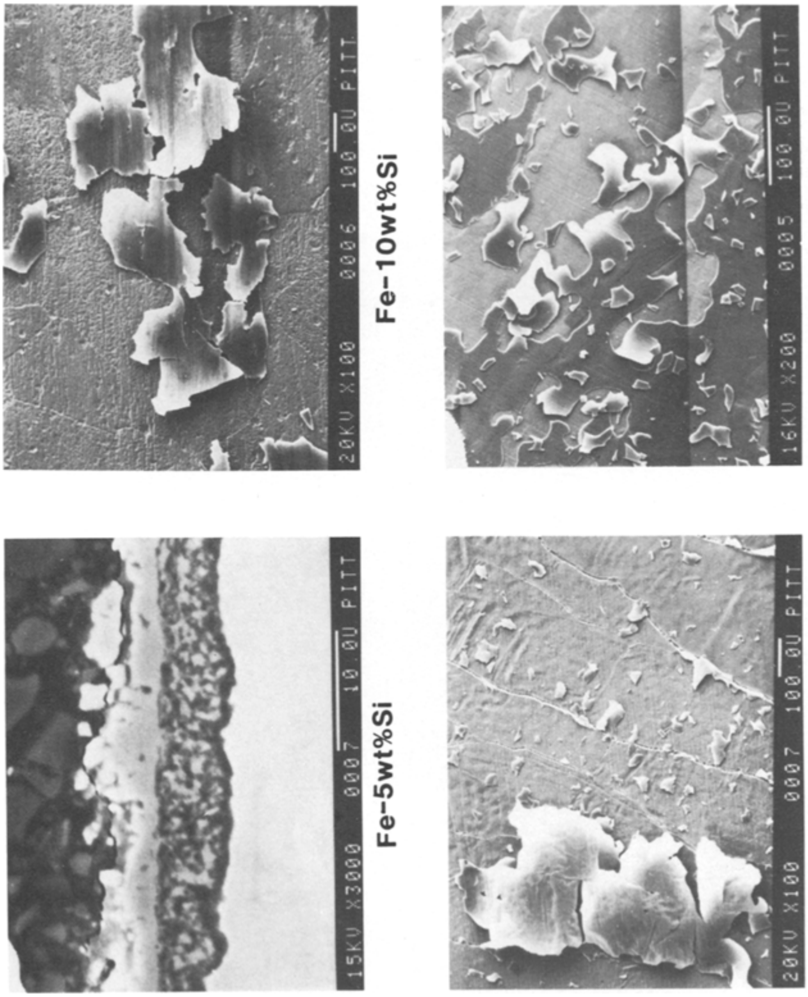

Fig. 5. Cross section of Fe–5Si and scale–gas interfaces for Fe–10, 14, and 20 Si oxidized in air for 1 week at 1000°C.

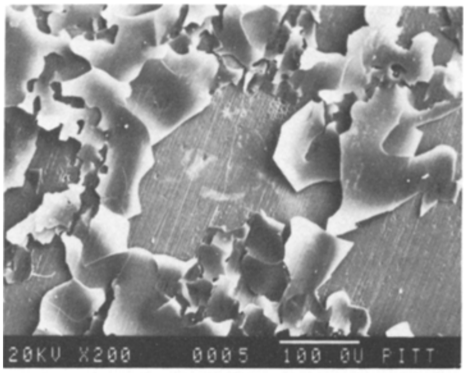

Fe-10wt%Si

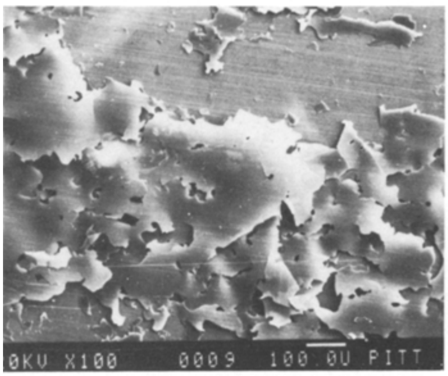

Fe-14wt%Si

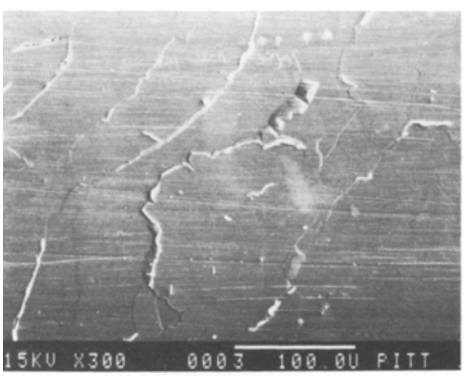

Fe-20wt%Si

Fig. 6. Scale–gas interface for three Fe–Si alloys oxidized in air for 1 week at 900°C.

of Fe_2O_3 and an inner layer of Fe_2SiO_4 dispersed in Fe_2O_3. The scale on Fe–20Si consists of a thin inner layer of cristobalite covered with Fe_2O_3. Figure 4 shows that the scale on Fe–14Si has completely spalled on cooling but examination of the spalled oxide indicated a morphology similar to Fe–20Si. An additional feature, observed only for Fe–14Si, was the presence of facetted voids in the alloy substrate with filaments of SiO_2 growing out from their base.

Figure 5 shows the cross section of Fe–5Si and surfaces of Fe–10, 14, and 20Si after oxidation at 1000°C in air for 1 week. The scale on Fe–5Si is similar to that observed at 1100°C with an outer layer of Fe_2O_3 and inner layer with a significant amount of Fe_2SiO_4. However, both layers are considerably thinner at 1000°C. The scale on the higher Si content alloys was mainly SiO_2 with no indication of Fe_2O_3 formation. The scales became smoother with increasing Si content but all showed considerable cracking on cooling.

Figure 6 shows the surface of three alloys oxidized at 900°C in air for 1 week. In all cases the scales were thin Si-rich oxide.

Figure 7 shows the spalled oxide and alloy substrate for Fe–14Si oxidized for 50 hr in air at 1100°C. The substrate contains facetted voids and globular particles, indicated by EDX analysis to be a pure oxide of iron. The origin of these particles, which did not change at longer oxidation times, is unclear. The underside of the spalled scale contains protrusions of SiO_2, containing small amounts of Fe, which appear to correspond to the voids in the substrate, and smooth areas of SiO_2. Analysis of the smooth areas by EDX analysis indicated a significant Fe content but this is believed to be due to generation of X-rays from the scale–gas interface, shown in Fig. 7 to be covered by crystallites of Fe_2O_3. It is significant that these Fe_2O_3 particles were not present after 1 hr of oxidation, so they are not the result of transient oxidation. Therefore, it appears that the SiO_2 layer, formed initially, is permeable to Fe. In order to investigate this phenomenon further, experiments involving preoxidation at low p_{O_2} and acoustic emission to detect scale cracking were performed.

Figure 8 shows weight change vs. time data for Fe–5Si and Fe–20Si oxidized for 1 week in tank argon (residual $p_{O_2} \simeq 10^{-4}$ atm) following which the atmosphere was changed to air without cooling the specimens. The oxidation rates for both alloys were quite low during the argon exposure but increased almost immediately when the atmosphere was changed to air. (The increase is not obvious for Fe–20Si because of the scale used in plotting Fig. 8.) The morphologies developed in the Ar and Ar → Air exposures are presented in Figs. 9 and 10. During the argon exposure both alloys developed a continuous SiO_2 (cristobalite) film (dark phase) overlaid with small amounts of Fe_2O_3. Upon switching to air, significant amounts of Fe_2O_3

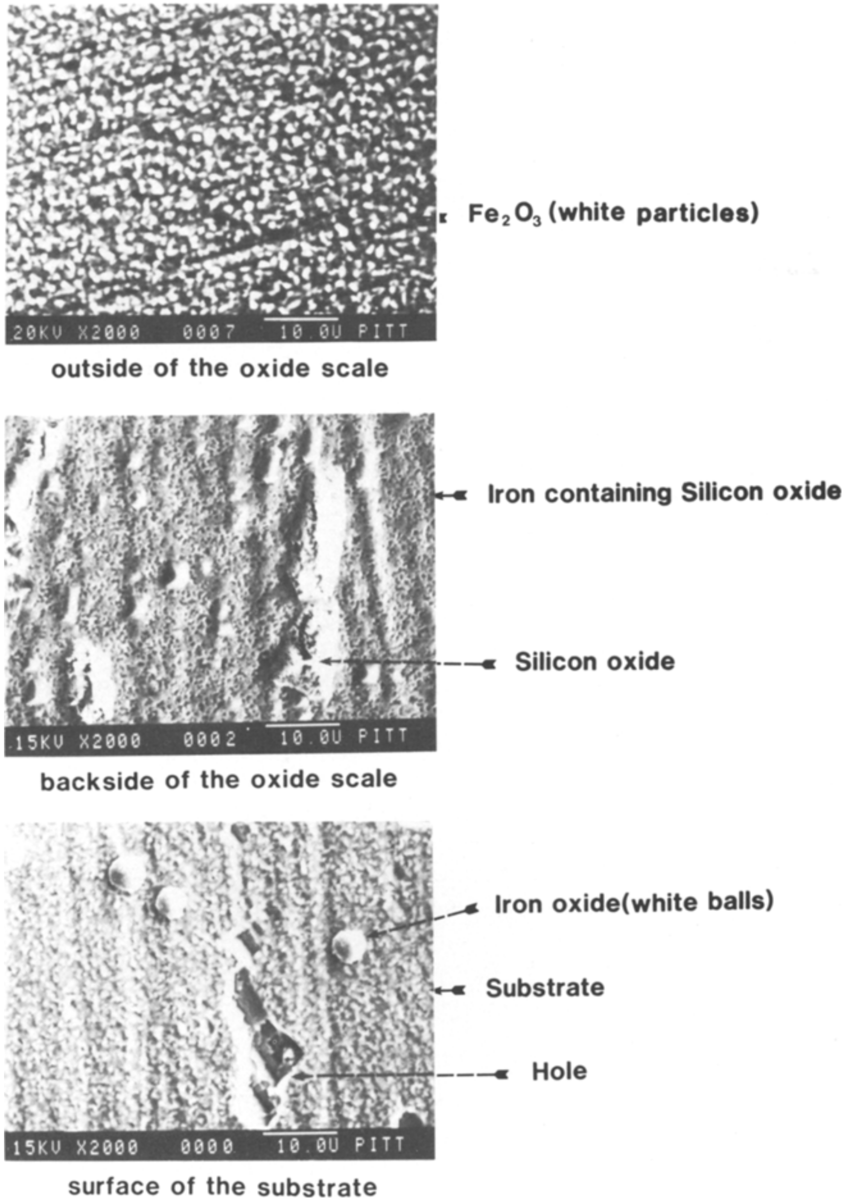

Fig. 7. Spalled oxide and alloy substrate for Fe–14Si oxidized in air for 50 hr at 1100°C.

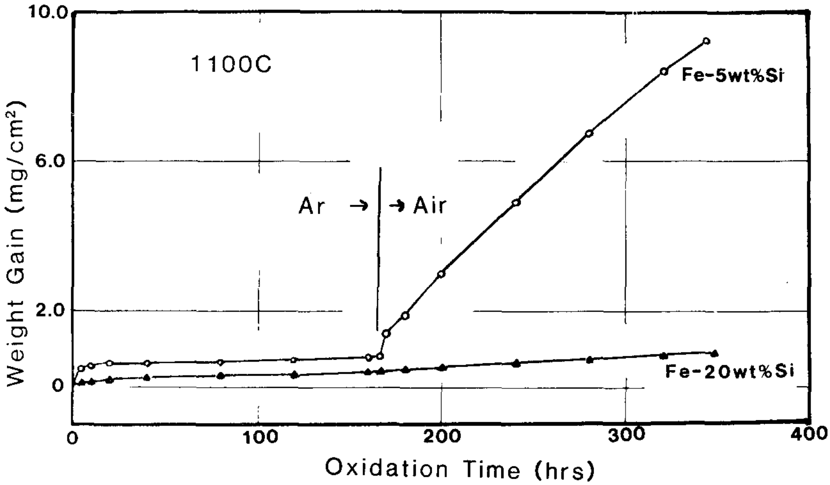

Fig. 8. Isothermal oxidation rates for Fe-5Si and Fe-20Si in tank argon ($p_{O_2} \approx 10^{-4}$ atm) followed by air at 1100°C.

began to form at the scale-gas interface, particularly for Fe-5Si. These data indicate that SiO_2 is permeable to Fe and that the permeation is more rapid at higher p_{O_2}. Furthermore, it appears that the permeation is associated with diffusion of un-ionized Fe through the SiO_2 since the measured diffusivity of Fe^{3+} in amorphous SiO_2 is comparable to that for O_2 in this temperature range[17] and, thus, is too low to account for the rapid growth of Fe_2O_3. Unfortunately, the diffusivity of Fe^{3+} in cristobalite is not available. The mechanism believed to operate in this case is illustrated schematically in Fig. 11. The driving force for the transport of Fe across a film of SiO_2 (presumed to be of essentially constant thickness) is the activity difference ($a'_{Fe}-a''_{Fe}$). For a given alloy composition a'_{Fe} is independent of the atmosphere, while a''_{Fe} decreases as p_{O_2} increases in the atmosphere as a result of the equilibrium

$$2Fe(s)+\frac{3}{2}O_2(g)=Fe_2O_3(s)$$

Therefore, the permeation rate of Fe through SiO_2 increases as p_{O_2} in the gas increases. For high p_{O_2}, where the Fe transport is rapid relative to the growth rate of the SiO_2 film, the weight change is essentially a linear function of the oxidation time. Conversely, for a fixed p_{O_2} in the gas, a''_{Fe} is constant, so the permeation rate of Fe through SiO_2 will increase as a'_{Fe} increases, e.g., Fe-5Si vs. Fe-20Si. Significant transport through SiO_2 of a metallic element with an oxide less stable than SiO_2 has been reported previously for the oxidation of Cu-Si[18] and Ni-Si[19] alloys.

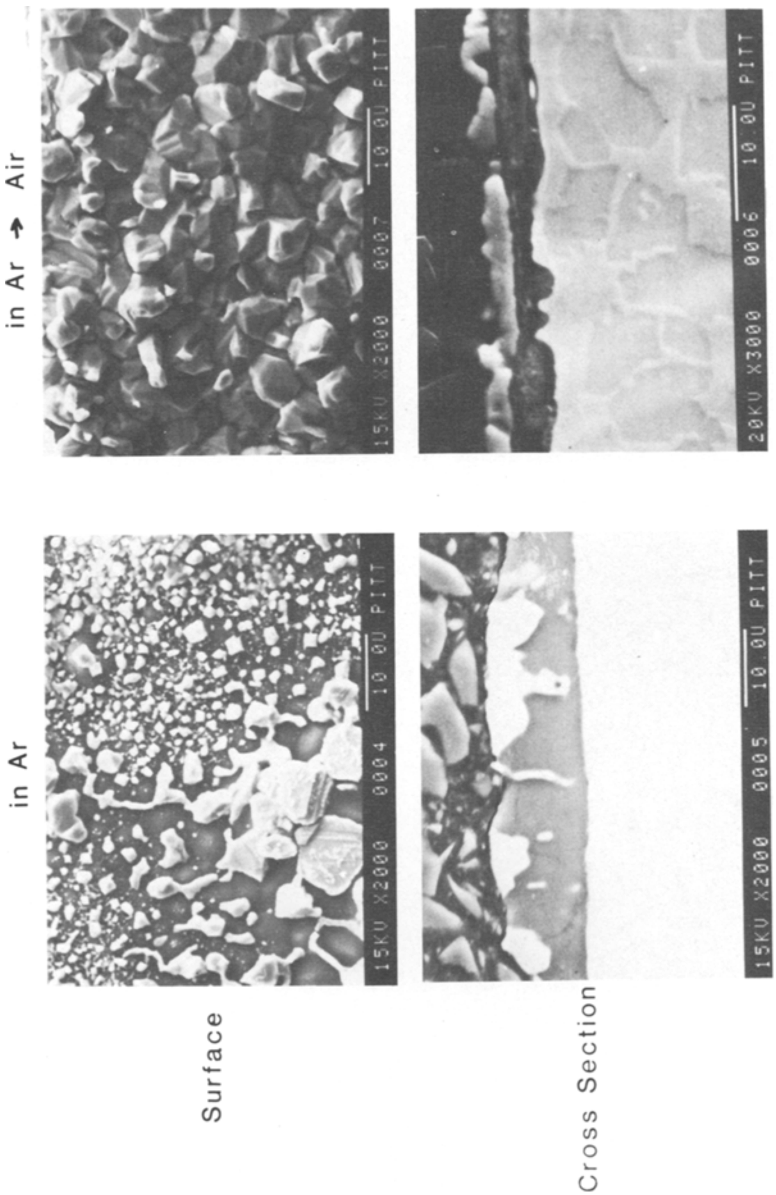

Fig. 9. Scale–gas interface and cross section of Fe–5Si oxidized in argon for 1 week followed by air for 1 week at 1100°C.

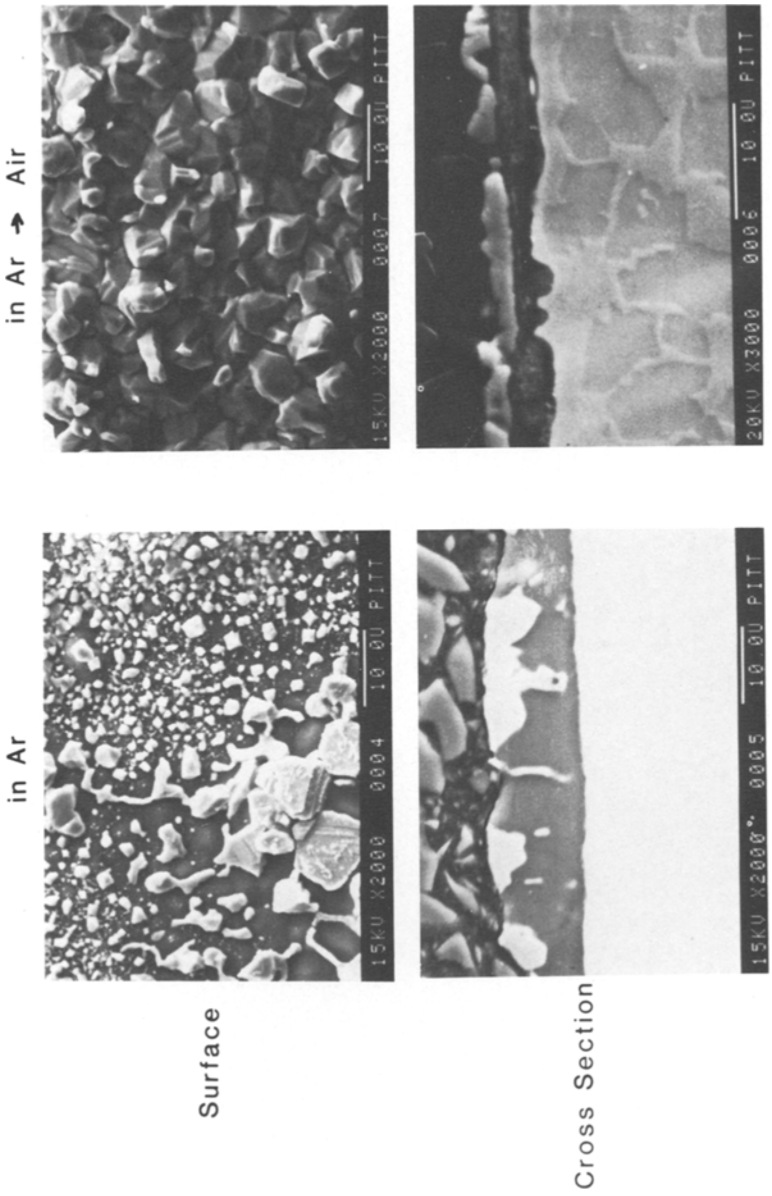

Fig. 10. Scale-gas interface and cross section of Fe-20Si oxidized in argon for 1 week and in argon for 1 week followed by air for 1 week at 1100°C.

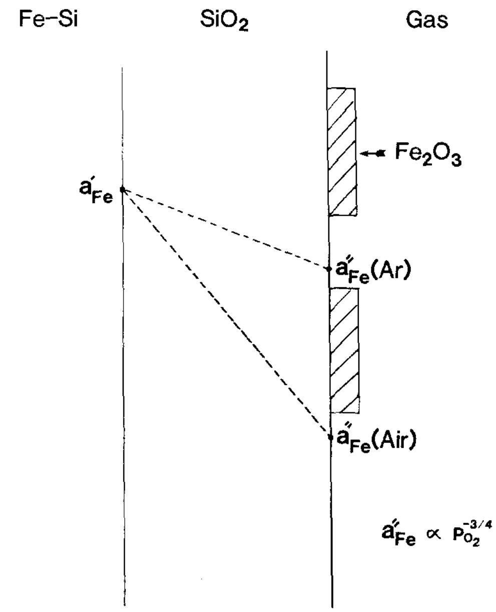

Fig. 11. Schematic diagram showing the gradients in iron activity across a SiO_2 film on Fe–Si in a high p_{O_2} (air) and low p_{O_2} (argon) atmosphere.

Additional experiments were performed using acoustic emission to ascertain whether the growth of Fe_2O_3 on top of a SiO_2 layer could be associated with cracking of the layer during isothermal oxidation. Figure 12 shows the AE counts measured from three alloys during a 4-hr oxidation at 1100°C and subsequent cooling. The counts during isothermal oxidation are only background. Similarly, Fig. 13 shows that only background counts are observed when Fe–14Si and Fe–20Si are oxidized for 50 hr. Therefore, there is no indication of scale cracking associated with the formation of Fe_2O_3.

The oxidation mechanisms in air at 1100°C of the four alloys are summarized in the schematic diagrams of Fig. 14. The initial stage of oxidation of Fe–5Si ($N_{Si} = 0.095$) involves areas covered with a layered scale with an outer Fe_2O_3 and inner $Fe_2SiO_4 + Fe_2O_3$ layer separated by thin areas of SiO_2. However, the Si content of the alloy is too low to maintain the SiO_2 film, and at steady state the two-layered scale covers the entire surface. This observation is not in agreement with the predictions of Atkinson[10] that $N_{si} \simeq 0.05$ should be sufficient in this temperature range to develop and maintain a continuous layer of SiO_2. The reason for this is that Atkinson's predictions, made primarily for applications in low p_{O_2}

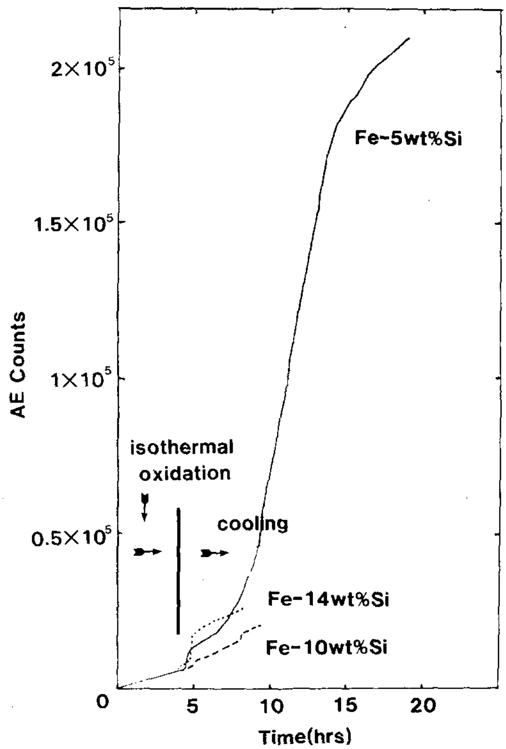

Fig. 12. Acoustic emission counts from Fe-Si alloys during isothermal oxidation for 4 hr in air at 1100°C and during subsequent cooling in the furnace.

CO-CO_2 atmospheres, do not account for the growth rate of the transient Fe oxides. It was recently shown[20] that the critical solute concentration for the transition from internal to external oxidation of an element such as Si can increase markedly with increased growth rate of the transient oxides. In the present case continuous SiO_2 films did form on Fe-5Si in argon ($p_{O_2} \simeq 10^{-4}$ atm), where the transient oxidation rate was reduced. For Fe-10Si, the initial scale consists of larger areas of SiO_2 between islands of the two-layered scale that grow with continued exposure at 1100°C. At lower temperatures, the thin SiO_2 layer covers most of the surface for times greater than 1 week. At 1100°C the SiO_2 layer, which may have nucleated as vitreous oxide, was observed to be cristobalite after 4 hr and to transform to tridymite between 4 and 24 hr. This transformation was not observed in the weight change vs. time plot. However, a small effect would have been masked because of the significant contribution of Fe_2O_3 growth to the overall weight change. The scales formed initially on Fe-14Si and Fe-20Si were essentially

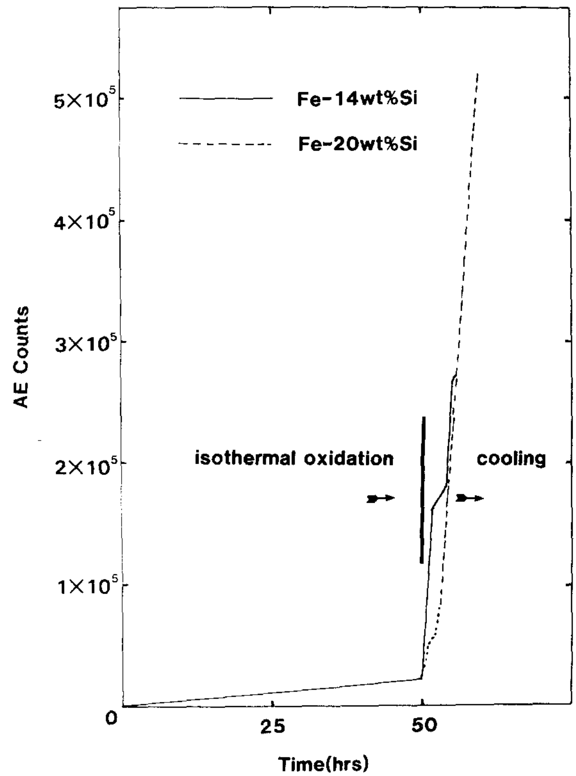

Fig. 13. Acoustic emission counts from Fe-Si alloys during isothermal oxidation for 50 hr in air at 1100°C and during subsequent cooling in the furnace.

pure SiO_2, which was identified as cristobalite for times from 4 hr to 1 week at 1100°C. With continued exposure, Fe_2O_3 formed at the scale-gas interface due to the outward diffusion of Fe, probably metallic, through the SiO_2 layer. This resulted in essentially linear oxidation kinetics, as the Fe was being transported through a SiO_2 layer of almost constant thickness. This oxidation process resulted in the formation of faceted voids in the alloy substrate for Fe–14Si by an undetermined mechanism.

Cyclic Oxidation

The oxidation morphologies (Figs. 3–7) and acoustic emission counts (Figs. 12 and 13) indicate significant cracking and spalling of the oxide scales during cooling after isothermal oxidation. Figure 15 shows weight change vs. the number of cycles for the cyclic oxidation of the four alloys in air at 900, 1000, and 1100°C. Above 900°C Fe–5 Si exhibited positive

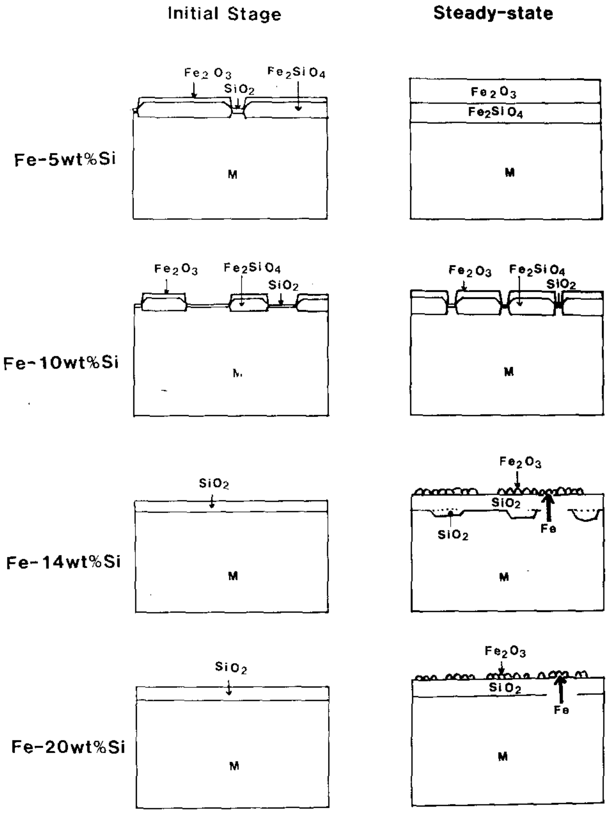

Fig. 14. Schematic diagram of the oxidation mechanism of Fe-Si alloys in air at 1100°C.

weight gains due to the rapid growth rate of Fe_2O_3 and little spalling, since the coefficients of thermal expansion for Fe-Si solid solutions[21] ($14.9–15.4 \times 10^{-6}\ °C^{-1}$) and Fe_2O_3[22] ($14.9 \times 10^{-6}\ °C^{-1}$) are closely matched. The Fe-10Si alloy showed a net weight loss at all temperatures, but at 1100°C is showed some periods of weight gain. The Fe-14Si alloy showed small weight changes at all three temperatures. However, these data are misleading because they are the result of a balance between significant scale spalling and scale growth. The Fe-20Si alloy gained weight at all three temperatures. However, at 1000 and 1100°C the specimens underwent a marked shape change and eventually fractured. The cause of this shape change was not determined, however, Fig. 1 indicates that this alloy undergoes a eutectoid transformation at 825°C, which may be responsible.

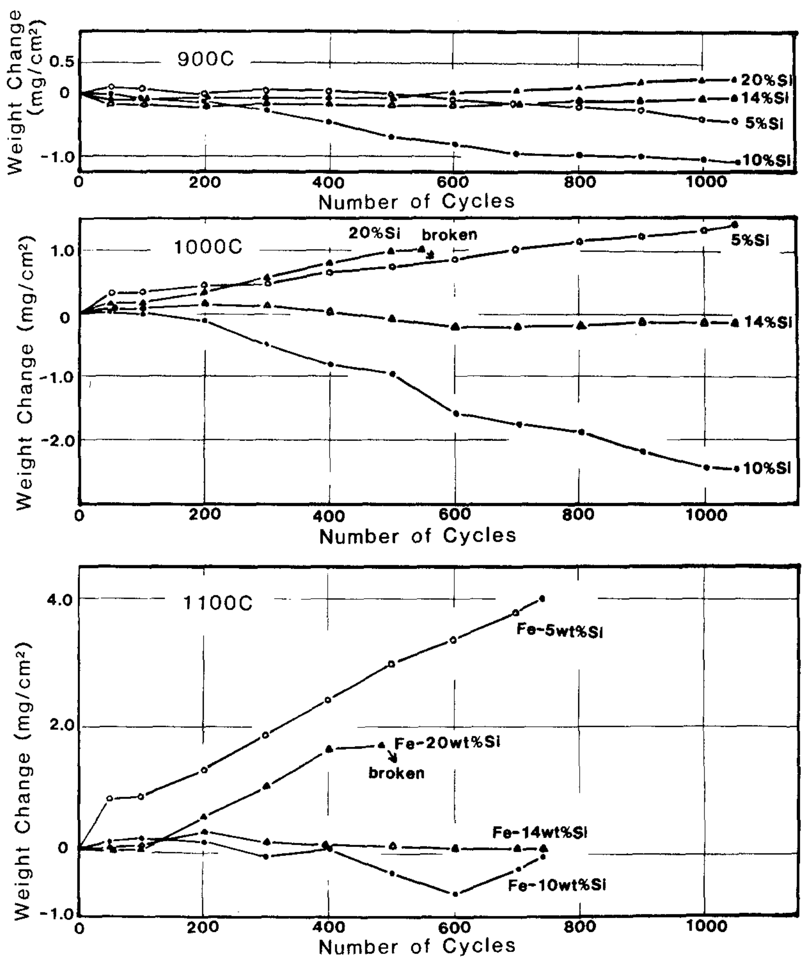

Fig. 15. Cyclic oxidation rates (weight change vs. number of cycles) for Fe–Si alloys in air.

The cristobalite films formed in argon at 1100°C were observed to be considerably more adherent than films of comparable thickness formed in air. The source of this difference has not been determined.

SUMMARY

The air oxidation rate of Fe–Si alloys decreased with increasing Si content (5–20 wt.%) at 900, 1000, and 1100°C. Alloys containing 10 wt.% Si or more oxidized slower than a typical Cr_2O_3-forming alloy (Fe–26Cr) due to the formation of an SiO_2 film. The oxidation kinetics were essentially linear after an initial period due to the outward permeation of Fe through a diffusion barrier (SiO_2) of nearly constant thickness to form Fe_2O_3 at the scale-gas interface. The Fe_2O_3 formation was not related to cracking of the SiO_2 layer. The alloys containing 10 and 14 wt.% Si showed significant scale spalling during cyclic oxidation. The alloy containing 20 wt.% Si gained weight during cyclic oxidation but underwent a shape change and eventually fractured at temperatures above 1000°C.

ACKNOWLEDGMENTS

The authors gratefully acknowledge the financial support of this work by the US-DOE under contract No. 19X-43346-C administered by Oak Ridge National Laboratory. The authors also acknowledge K. Andrew, E. Hewitt, and G. McManus for experimental assistance and Professors E. A. Gulbransen and F. S. Pettit for helpful discussions.

REFERENCES

1. T. Nakayama and M. Sugiyama, *J. Jpn. Inst. Met.* **23**, 534 (1959).
2. C. W. Tuck, *Corr. Sci.* **5**, 631 (1965).
3. R. Logani and W. W. Smeltzer, *Oxid. Met.* **1**, 3 (1969).
4. R. C. Logani and W. W. Smeltzer, *Oxid. Met.* **3**, 15 (1971).
5. R. C. Logani and W. W. Smeltzer, *Oxid, Met.* **3**, 279 (1971).
6. I. Svedung and N. G. Vannerberg, *Corr. Sci.* **14**, 391 (1974).
7. P. T. Moseley, G. Tappin, and J. C. Riviere, *Corr. Sci.* **22**, 69 (1982).
8. A. Schnaas and J. J. Grabke, *Oxid. Met.* **12**, 387 (1978).
9. G. M. Kim and G. H. Meier, "Breakdown Mechanisms of Preformed Al_2O_3, Cr_2O_3, and SiO_2 Scales in H_2-H_2O-H_2S Environments," University of Pittsburgh, Report on Martin-Marietta Subcontract No. 19X-43346-C, March 1987.
10. A. Atkinson, *Corr. Sci.* **22**, 87 (1982).
11. M. Hansen and K. Anderko, *Constitution of Binary Alloys*, 2nd ed. (McGraw-Hill, New York, 1958), p. 711.
12. G. V. Raynor and V. G. Rivlin, *Int. Met. Rev.* **30**, 181 (1985).
13. A. Ashary, G. H. Meier, and F. S. Pettit, *in High Temperature Protective Coatings*, S. C. Singhal, ed. (AIME, 1982), p. 105.
14. R. A. Perkins and G. H. Meier, in *High Temperature Materials Chemistry Vol. II*, Z. A. Munir and D. Cubicciotti, eds. (The Electrochemical Society, 1983), p. 176.
15. M. H. Davies, M. J. Simnad, and C. E. Birchenall, *J. Met.* **3**, 889 (1951).
16. D. Caplan and M. Cohen, *Nature* (Lond.) **205**, 690 (1965).
17. A. Atkinson and J. W. Gardner, *Corr. Sci.* **21**, 49 (1981).
18. J. Kapteijn, S. A. Couperus, and J. L. Meijering, *Acta Met.* **17**, 1311 (1969).
19. A. Ashary, G. H. Meier, and F. S. Pettit, *Advanced High Temperature Coating Systems Beyond Current State-of-the-Art Systems* University of Pittsburgh, Final Report on AFOSR Contract No. 80-0089, April 1986).
20. F. Gesmundo and F. Viani, *Oxid. Met.* **25**, 269 (1986).
21. Mechanical Properties of Metals and Alloys, Circular C447, U.S. Department of Commerce (1943), p. 284.
22. P. Hancock and R. E. Hurst, in *Advances in Corrosion Science and Technology*, R. W. Stahle and M. G. Fontana, eds. (Plenum Press, New York 1974), p. 1.